Available online at www.sciencedirect.com
SCIENCE DIRECT
Journal of the European Ceramic Society 26 (2006) 2719–2726
www.elsevier.com/locate/jeurceramsoc

Characterization of α-Al_2O_3–$(Al–Si)_3Ti$ composites

Shaul Avraham [a,*], Peter Beyer [b,1], Rolf Janssen [b], Nils Claussen [b], Wayne D. Kaplan [a]

[a] *Department of Materials Engineering, Technion-Israel Institute of Technology, 32000 Haifa, Israel*
[b] *Advanced Ceramic Group, Technical University Hamburg-Harburg, D-21071 Hamburg, Germany*

Received 18 January 2005; received in revised form 6 June 2005; accepted 10 June 2005
Available online 8 August 2005

Abstract

The reactions that take place during the formation of ceramic matrix composites that are based on α-Al_2O_3–$(Al–Si)_3Ti$ interpenetrating networks were analysed. A reactive preform was pressure infiltrated with an Al–Si alloy. After pressure infiltration, the composite did not react in a full manner and further thermal annealing was required. The reduction of TiO_2 by the liquid Al–Si alloy results in the formation of $(Al-Si)_3Ti$ ($Al_{60}Si_{12}Ti_{28}$). The formation of $(Al–Si)_3Ti$ is governed by the consumption of TiO that is formed as an intermediate phase during the reduction of TiO_2.

Keywords: Al_2O_3; TiO_2; $(Al–Si)_3Ti$; Composites; Microstructure

1. Introduction

Ceramic matrix composites (CMC) have a wide range of applications due to increased fracture toughness, strength and thermal shock resistance compared to monolithic materials.[1,2] The advantages of CMC are derived from their unique microstructures. In some cases, each phase percolates throughout the microstructure and an interpenetrating network (IPN) microstructure is achieved. One of the reasons for the enhanced mechanical properties is the role of crack-bridging by ductile metal ligaments.[3]

Aluminide intermetallics (FeAl, $AlNb_3$ and $AlTi_3$) are attractive for high temperature applications due to their high melting points ($T_m > 1000\,^\circ C$) and relatively low densities. The incorporation of aluminide intermetallics as reinforcing phases in a ceramic matrix may improve the potential applications of such composites at high temperatures.[4]

α-Al_2O_3 is among the most extensively studied and applied ceramics.[5] One processing route for α-Al_2O_3 based CMC is via the reduction of a reactant oxide component by Al. This can be achieved by several different methods.[4,6,7] An optional route for producing near net shape CMC is the infiltrated Al_2O_3–Al_3X alloy (i-3A) technique.[8,9] The i-3A process is based on pressure infiltration of liquid Al-alloys into a porous preform, which is composed of Al_2O_3 and a reactive oxide (such as TiO_2, Nb_2O_5 or Fe_2O_3). In TiO_2 based CMC, a reduction reaction takes place, where Al_3Ti is produced by the reduction of TiO_2 by Al according to:[10,11]

$$3TiO_2 + 13Al \rightarrow \cdots \rightarrow 3Al_3Ti + 2\alpha\text{-}Al_2O_3 \quad (1)$$

The TiO_2 reduction reaction is generalized due to the fact that it is divided into sub-reactions that take place in the solid and liquid phase over a wide temperature range.[10,11] The intermediate phases that were observed as a result of the different heat treatments include: titanium oxides (TiO, Ti_2O_3), Al–Ti intermetallics (TiAl, Ti_3Al) and γ-Al_2O_3.[10,11]

This work probes the unique microstructure and various reactions that take place during the different stages of production of partially reinforced lightweight structural components, based on Al_2O_3–TiO_2 preforms that were infiltrated by commercial Al-alloys.

* Corresponding author.
E-mail address: shaula@tx.technion.ac.il (S. Avraham).
[1] Present address: Meister Abrasives AG, Industriestr. 10, CH-8450 Andelfingen, Switzerland.

0955-2219/$ – see front matter © 2005 Elsevier Ltd. All rights reserved.
doi:10.1016/j.jeurceramsoc.2005.06.024

Table 1
Sample composition and heat treatments

Sample Id.	Al_2O_3 (vol.%)	TiO_2 (vol.%)	Al-alloy (vol.%)	Annealing process
E2	25.5	25.5	49	As-infiltrated
B1	25.5	25.5	49	650 °C, 3 h
B2	25.5	25.5	49	1000 °C, 20 min

2. Experimental methods

2.1. Materials

The ceramic powders that were used in the production of the samples were a mixture of α-Al_2O_3 (Alcoa CT 1200SG) and TiO_2 (Riedel de Hean 14021). The CMC samples were prepared by a three-step process: preform processing, pressure infiltration and thermal annealing. The two initial stages are described elsewhere.[9] The milled ceramic powder was compacted (75 MPa uniaxial pressing) and partially sintered in air (1 °C/min heating to 700 °C followed by 3 °C/min heating up to 1150 °C). A commercial Al-alloy which contained 12 wt.% Si [GB-AlSi12(Cu), German Standard] was heated to 750 °C and was pressure infiltrated (39 MPa) into the preheated (600 °C) ceramic preform (40 mm × 40 mm × 5 mm).

After pressure infiltration, thermal treatments were conducted in a box furnace at a temperature of 650 °C for 3 h and 1000 °C for 20 min. The heat treatments were carried out using a heating rate of 15 °C/min. Table 1 summarizes the CMC sample composition and various heat treatments.

2.2. Characterization methods

Differential thermal analysis (DTA) was conducted on samples weighing ≈50 mg. The measurements were conducted using a Perkin-Elmer DTA (system 7/4) with a maximum working temperature of 1500 °C. The scan rate of the pressed powder samples was 7 °C/min, and the air flow was 2 cc/min (air flow was used to simulate the firing stage of the pressed powder). DTA analysis of the as-infiltrated CMC was conducted under air (2 cc/min) and argon flow (2 cc/min, 99.9%). The scan rate was 15 °C/min until a maximum temperature of 1100 °C was reached.

The microstructure of the samples was investigated using X-ray diffraction (XRD), scanning electron microscopy (SEM) and transmission electron microscopy (TEM) techniques. XRD measurements were conducted in a conventional X-ray automatic powder diffractometer (PW-3020 goniometer, Philips, Netherlands) using Cu Kα, operated at 40 mA and 40 kV. The XRD step scans from the E2, B1 and B2 samples were acquired from 20 to 125° with a step size of 0.05° and a dwell time of 6 s per step.

Samples for SEM were mounted (if necessary) in epoxy resin to prevent any possible damage to the specimens during specimen preparation. The specimens were prepared by diamond disk cutting, diamond polishing of the cross-section (0.25 μm surface finish) and carbon coating. No etching process was applied. SEM was conducted using a FEI XL-30 microscope, equipped with an energy dispersive spectrometer (EDS) (6506, Oxford Instruments, UK) for microanalysis of the sample (elemental detection limited to $Z > 4$). The accelerating voltage during the analysis was 10 kV and the working distance was 10.5 mm. High resolution SEM was conducted on a LEO 982 Gemini microscope equipped with a field emission gun (FEG-SEM), at 3 kV and a working distance of 3–5 mm.

Plan-view TEM samples were prepared by ultrasonic cutting, mechanical polishing and dimpling, followed by ion-milling with Ar at 5 kV until perforation. A thin carbon coating was applied to prevent charging under the electron beam. The study of the microstructure was conducted using a JEOL 2000FX TEM at 200 kV equipped with an EDS system (Link AN10000, $Z > 10$ Oxford Instruments, Oxford, England).

3. Results

3.1. Pressed and preform samples

Fig. 1a presents a high magnification secondary electron (SE) SEM micrograph of the pressed powder sample. The identity of the different phases was confirmed by EDS. It is apparent that the grain size distribution is bi-modal, with micron-size Al_2O_3 grains and sub-micron grains of TiO_2. The function of the powder pressing stage is to shape the

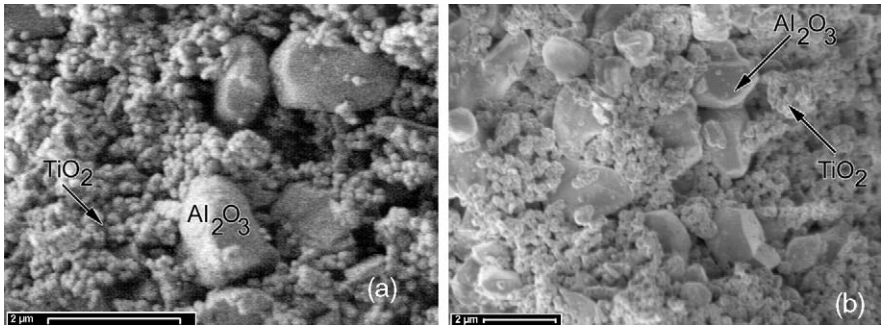

Fig. 1. Secondary electron (SE) SEM micrographs of (a) the pressed sample, and (b) the fired preform.

sample, and to create the initial contact between grains that will be enhanced during the firing stage.

Fig. 1b presents a SE SEM micrograph of the *fired* preform. The bi-modal size distribution is clearly visible. The contact area between the TiO_2 grains is increased. No clear tendency of enhanced contact area between the alumina grains can be seen.

3.2. CMC samples

Fig. 2 presents the DTA curve recorded during heating of the as-infiltrated CMC sample (E2). Under argon, a sharp endothermic peak can be observed during heating at ≈580 °C (marked as *a* in Fig. 2). This peak results from re-melting of the Al-alloy used for pressure infiltration. In addition, two subsequent exothermic peaks are observed at 614 °C (marked as *b* Fig. 2) and at 723 °C (marked as *d* Fig. 2). In air, the temperature of the endothermic melting and the first exothermic peak shifts by 6–20 °C. The temperature of the second exothermic peak decreases by 20 °C. The use of Ar as a protective gas prevents oxidation, which is the cause for the differences between the two DTA curves. Points *c* and *e* in Fig. 2 represent the temperatures at which thermal annealing of infiltrated CMC samples was conducted (*c* for samples B1 and *e* for sample B2, see Table 1).

The XRD results from the samples are presented in Fig. 3. The as-infiltrated sample (E2) contains α-Al_2O_3, Al and TiO_2. The presence of Si results from the depletion of the Si containing Al-alloy, due to the low solubility of Si in Al.

Sample B1 was infiltrated using Al-alloy 231 and annealed at 650 °C for 3 h. As expected, the sample is partially composed of α-Al_2O_3. The reduction of TiO_2 intensifies, and results in a large amount of $(Al–Si)_3Ti$. The presence of this specific phase was confirmed by EDS in SEM, and TEM combined with selected area diffraction (SAD). The sample contains alumina, including the initial alumina powder and secondary alumina, formed during the reduction of TiO_2 by Al. The presence of residual Al is evident in the XRD pattern. Residual TiO_2 was not detected.

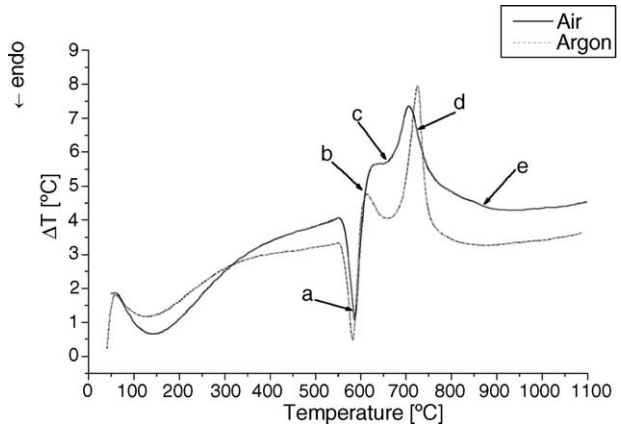

Fig. 2. DTA curve (during heating) of the as-infiltrated CMC.

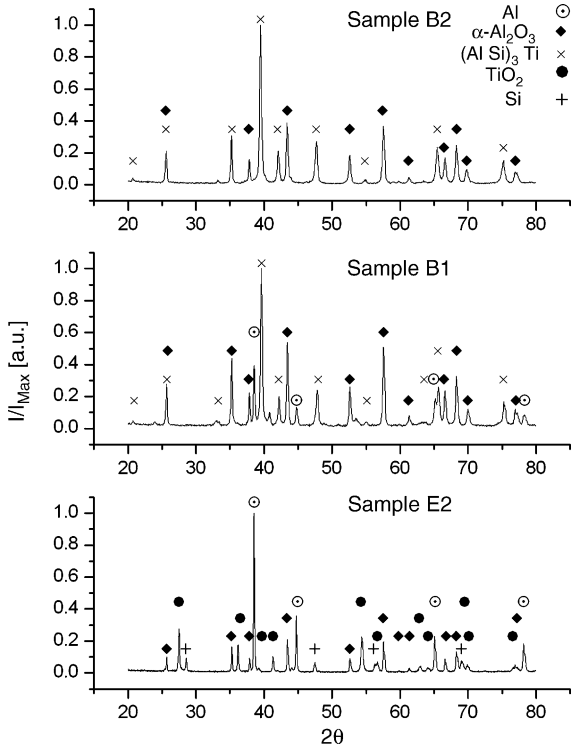

Fig. 3. XRD diffraction patterns of samples E2, B1 and B2.

Sample B2 was infiltrated using Al-alloy 231 and annealed at 1000 °C for 20 min. From Fig. 3, it is clear that the reduction reaction is complete. The higher annealing temperature resulted in a fully reacted $(Al–Si)_3Ti$-α–Al_2O_3 sample without any residual phases.

It should be noted that a significant shift (up to $\Delta 2\theta = 0.9°$) was observed in the position of the $(Al–Si)_3Ti$ XRD reflections in samples B1 and B2, compared to the standard Al_3Ti reflections.[12] The change in the reflection position is attributed to lattice parameter changes due to the formation of an $(Al–Si)_3Ti$ intermetallic phase.

Fig. 4 is a backscattered electron (BSE) SEM micrograph of the microstructure of the as-infiltrated CMC (sample E2). As mentioned previously, TiO_2 and Al_2O_3 are present in the composite. TiO_2 agglomerates were rarely observed.

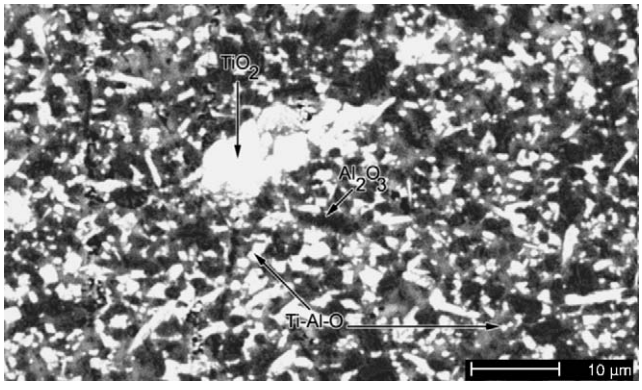

Fig. 4. BSE micrograph of the CMC after infiltration (sample E2).

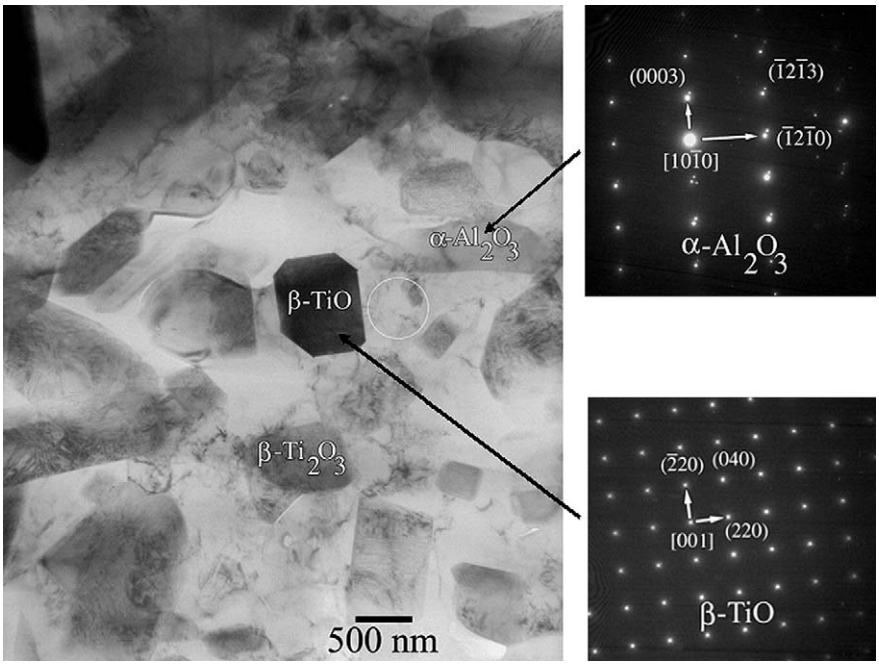

Fig. 5. BF TEM micrograph of sample E2.

Al–Ti–O related precipitates are visible. EDS microanalysis was used to determine the identity of the phases.

TEM analysis confirmed the complex nature of the reactions that take place during the formation of the CMC. Fig. 5 presents a bright field (BF) TEM micrograph of sample E2 (as-infiltrated by Al-alloy 231). The presence of an α-Al_2O_3 grain with a mean diameter of ≈1.5 μm was confirmed by EDS and SAD. Based on the large dimensions of the particle, it was concluded that the α-Al_2O_3 grain originated from the initial alumina powder that was used in the preform preparation procedure.

The TiO_2 phase is reduced and transformed into a series of TiO polymorphs (α, β and γ) and β-Ti_2O_3. The formation of Ti_2O_3 is not surprising due to the fact that it was previously detected during reduction of TiO_2 by Al[10] and the complex nature of the Ti–O binary phase diagram.[13] The presence of β-TiO and β-Ti_2O_3 was confirmed by SAD. The ceramic oxides are embedded in the Al matrix (bright contrast), which was identified by EDS.

The phases in the Al matrix were identified using SAD (Fig. 6). The contrast of selected regions of the SAD was altered for presentation purposes. The measured *d*-spacing (see Table 2) implies that the matrix is composed of Al, α-Al_2O_3 and γ-Al_2O_3. The observed smearing of the ring pattern is caused by a size distribution among the inspected grains. In addition, a series of diffraction spots are visible, resulting from the presence of off-zone axis crystals.

A BSE SEM micrograph of the B1 sample is presented in Fig. 7. The initial phases that were used for the preparation of the CMC are visible: Al, Al_2O_3 and TiO_2. The circled region marked on the micrograph is abnormally enriched (compared to the general microstructure) with titanium oxides. The main product of the reduction reaction is found to be the Al_3Ti derivative, $(Al–Si)_3Ti$ and small amounts of residual phases ($CuAl_2$, $AlSi_7Ti_4$). The $CuAl_2$ intermetallic formed as a result of 1.2 wt.% Cu in the Al-alloy that was used.

Analysis of the dark grains in Fig. 7 showed that they could be divided into two groups: alumina grains and fine alumina particles embedded in the Al matrix (based on EDS results).

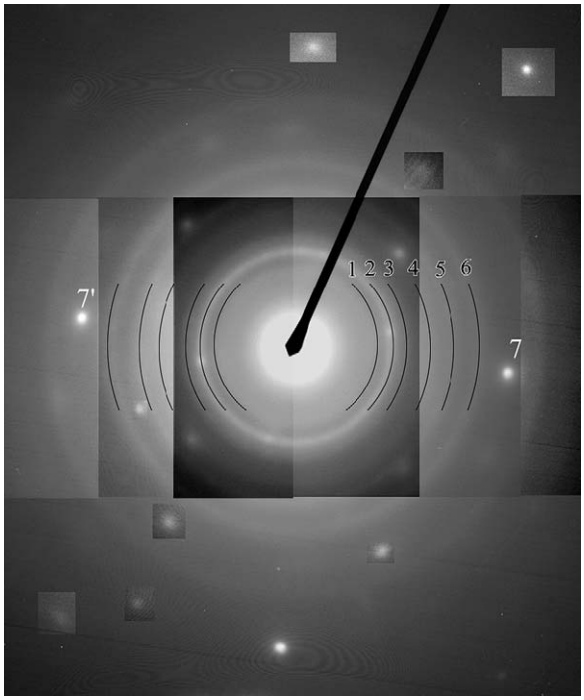

Fig. 6. SAD acquired from marked area in Fig. 5.

Table 2
Observed reflections from Al–O matrix ($d > 0.8$ Å)

	Observed d space (Å)	Phase	Plane
1	2.270	γ-Al_2O_3	(2 2 2)
2	1.931	γ-Al_2O_3	(0 0 4)
		α-Al_2O_3	(2 0 $\bar{2}$ 2)
3	1.680	γ-Al_2O_3	(2 4 2)
4	1.368	α-Al_2O_3	(3 0 $\bar{3}$ 0)
		γ-Al_2O_3	(4 4 0)
5	1.182	α-Al_2O_3	(2 2 $\bar{4}$ 0)
		Al	(4 0 0)
6	1.002	α-Al_2O_3	(0 4 $\bar{4}$ 2)
		γ-Al_2O_3	(8 0 0)
7	0.867	α-Al_2O_3	(0 4 $\bar{4}$ 8)
		γ-Al_2O_3	(5 7 3)

The large alumina grains correlate in size to the initial alumina phase that was used to form the ceramic preform. EDS measurements of the Al network detected the presence of large amounts of oxygen, since the Al network contains fine alumina particles. The presence of the fine Al_2O_3 particles is attributed to the formation of alumina as a by-product of the reduction reaction that takes place between the infiltrating Al-alloy and the reactive phases that compose the preform (TiO_2 and TiO). Si was detected during the analysis of the Al–Al_2O_3 regions. This is probably due to the depletion of the Al-alloy during cooling.

The bright regions in Fig. 7 can be divided into three groups: large grains, course precipitates and fine structured precipitates. XRD analysis showed that the large grains are an Al_3Ti derivative. EDS analysis revealed that the Si content in this phase is significant ($Al_{60.62}Si_{10.56}Ti_{28.81}$). The elemental composition is comparable to $Al_{60}Si_{15}Ti_{25}$.[14] The bright

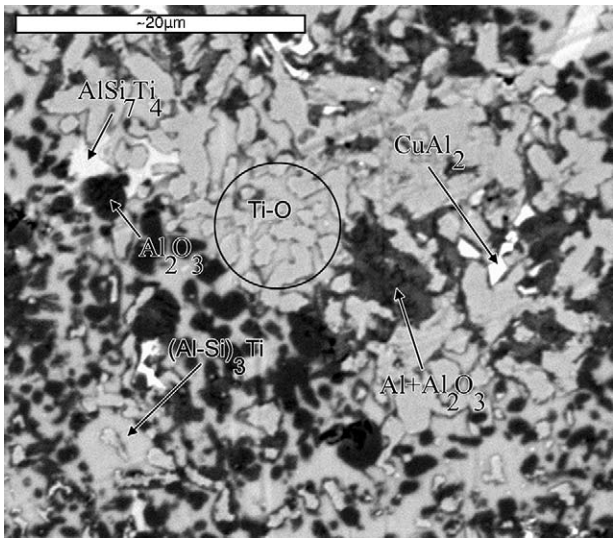

Fig. 7. BSE micrograph of sample B1.

coarse precipitates are titanium oxides of different compositions; stoichiometric TiO_2 and TiO were identified by EDS analysis. The fine precipitates were found to be composed of Al, Ti and Si, but no definite phase identification could be achieved via SEM-EDS. Open porosity is present at the sample surface. The results of the EDS analysis imply that closed porosity is present in the sample.

A BF TEM micrograph of the B1 sample is presented in Fig. 8. The presence of α-Al_2O_3 was confirmed by SAD. The dimensions of the grain suggests that the grain's origin is the initial alumina powder. Additional α-Al_2O_3 grains are evident in the micrograph. The mean grain diameter of the

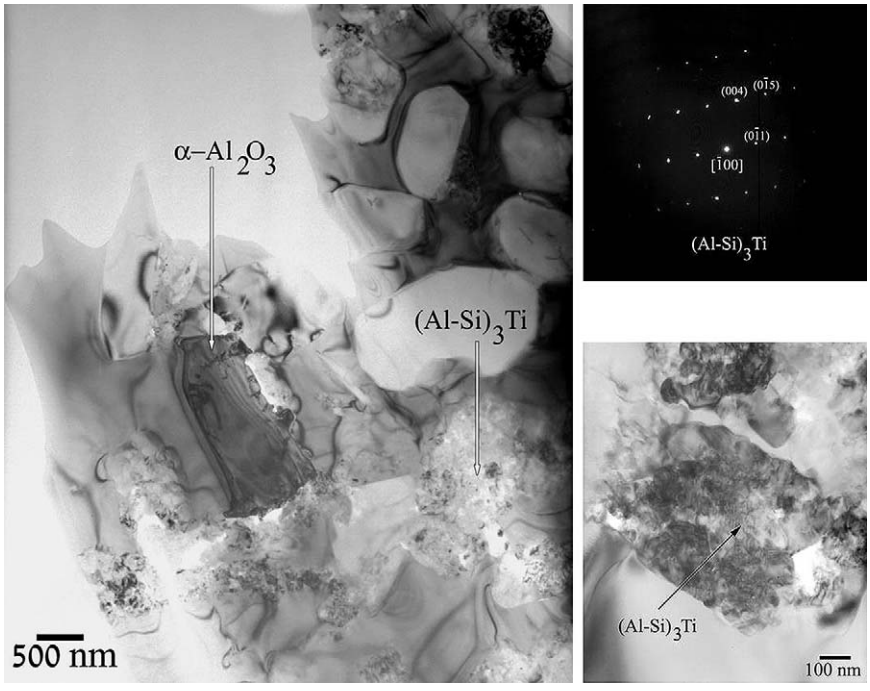

Fig. 8. BF TEM micrograph from sample B1. The insert is a magnified view and a SAD pattern of the $(Al–Si)_3Ti$ grain.

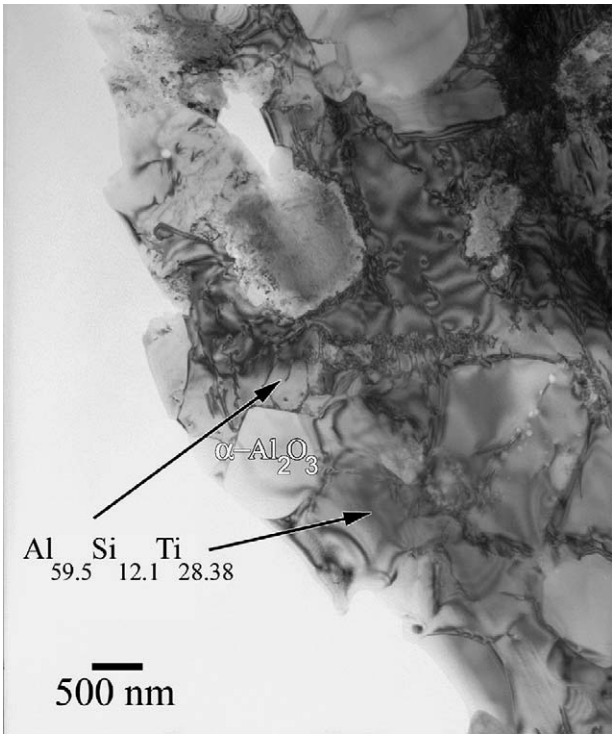

Fig. 9. BF TEM micrograph from sample B1.

observed α-Al_2O_3 is ≈1.4 μm. The fine structured region (shown in the insert) was confirmed by EDS analysis to be composed of an Al–Ti–Si intermetallic phase. SAD from the fine structured area revealed the crystallographic nature of the phase, which was found to be a variation of Al_3Ti, which contains relatively large amounts of Si.

Fig. 9 presents a BF TEM micrograph of the microstructure of the $(Al–Si)_3Ti$ intermetallic network. Quantitative EDS measurements in scanning transmission electron microscopy (STEM) mode revealed that the composition of the intermetallic is $Al_{59.5}Si_{12.1}Ti_{28.38}$, similar to $Al_{60}Si_{15}Ti_{25}$.[14]

A BSE SEM micrograph of the B2 sample is presented in Fig. 10. A homogeneously dispersed interpenetrating microstructure of Al_2O_3 and $(Al–Si)_3Ti$ is evident. EDS analysis showed that the Si content in this phase is similar to the previously (sample B1) measured elemental content ($Al_{60.62}Si_{10.56}Ti_{28.81}$). In addition, TiO_2 and TiO grains were detected. This is in correlation with the reduction reaction reactants and intermediate products. Alloying elements, such as Mg and Fe, were found in several cases. In all cases, there is a presence of silicon in the $(Al–Si)_3Ti$ intermetallic phase. Porosity was observed at the surface of the sample.

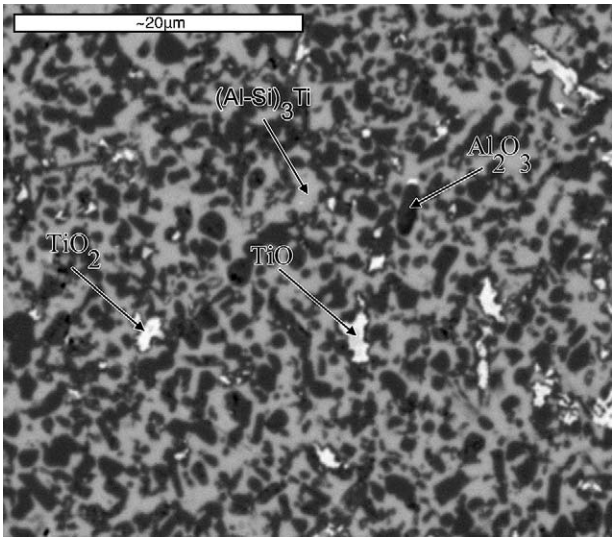

Fig. 10. BSE micrograph of sample B2.

4. Discussion

4.1. Pressed and preform samples

The pressed powder body is composed of TiO_2 and α-Al_2O_3 powders. TiO_2 plays a major role in the processing route, since it is the reactive oxide that is consumed in the reduction reaction that eventually produces the intermetallic phase. One of the functions of α-Al_2O_3, among others, is to serve as a diluting phase. A high volumetric fraction of TiO_2 can result in an uncontrolled exothermic reaction that can result in a large degree of residual porosity.

The effect of firing on the preform body can be deduced by comparing Fig. 1a and b. The sub-micron size grains tend to neck and increase the contact area between grains. The firing stage results in surface diffusion that promotes mass deposition at the neck area between the ceramic powder particles (in our case, α-Al_2O_3 and TiO_2 grains).[15] At the end of the firing stage, the contact area between the TiO_2 particles (neck area) is increased, and the fired preform has an increased strength and can withstand the pressure infiltration process.[15]

4.2. CMC phase formation

4.2.1. Phase transition during the pressure infiltration process

The ceramic preform that is ready for pressure infiltration is composed of α-Al_2O_3 and TiO_2 powder. The low density of the preform after firing (≈50%) results in a high specific surface area. This increases the reactivity of the preform. Increased specific surface area results in increased contact between the Al-alloy and the reactive oxide (TiO_2) during pressure infiltration.

It appears that the effective contact angle of the Al–Si alloy during infiltration is higher than the critical contact angle (≈50°) for spontaneous infiltration into a non-cylindrical porosity.[16] It should be noted that the final contact angle at 700 °C of pure Al on α-Al_2O_3 and on TiO_2 is, 101°[17] and >150°,[18] respectively.

During infiltration, the preform is heated to 600 °C. The molten alloy is heated to 750 °C and forced into the perform.

From XRD (sample E2, Fig. 3) and SEM results (Fig. 4), the reduction reaction during infiltration is partial. In addition to α-Al_2O_3 and unreacted TiO_2, the E2 sample contains residual Al and Si. The reduction reaction of TiO_2 by the Al–Si alloy does not take place, and additional thermal annealing is required.

4.2.2. Phase transition during thermal annealing

During thermal annealing, as the temperature reaches 580 °C (see Fig. 2, stage *a*), the Al–Si alloy is remelted. The melting temperature is similar to the value measured by Bayer et al.[9] and Hsu et al.[19] who analysed pressure infiltration of an Al-alloy into a pure TiO_2 preform (33 vol.%). The apparent melting temperature of the alloy which was measured here is lower than that of pure Al, which is a direct consequence of the initial Si content (10.5–13.5 at.%) in the alloy. The Al–Si phase diagram has a eutectic, at 12.2 at.% Si and ≈577 °C,[20] which is similar to the value measured here. Liquid state reactions ($T \approx 670$ °C) between *pure* Al and TiO_2 results in the formation of γ-Al_2O_3 and TiO.[11]

As the heating proceeds to ≈614 °C (see Fig. 2, stage *b*), an exothermic peak is detected. This peak is attributed to the reduction of TiO_2 by liquid Al, resulting in the formation of titanium oxides (Figs. 7 and 5) and α-Al_2O_3. $(Al–Si)_3Ti$ (see Fig. 9) is apparent at this stage. TiO_2 is still present in major quantities (see Fig. 3, sample B1). The intensity of the characteristic XRD reflection of Si decreases, which is attributed to the incorporation of Si into Al_3Ti and the formation of $(Al–Si)_3Ti$. The temperature of the reaction is low compared to the temperature measured by Feng et al.[11] This results from the fact that the melting point of the Al–Si alloy is lower than the melting point of pure Al ($\Delta T \approx 100$ °C).

$(Al–Si)_3Ti$ is formed to some extent during the annealing process, but its formation is centered at 723 °C (stage *d*, Fig. 2) and completes at 870 °C (stage *e*, Fig. 2). Above this temperature, no major quantities of TiO_2 can be observed (sample B2, Fig. 3).

The DTA results can be compared with the work of Hsu et al.,[19] who fabricated an in situ $Al_2O_3/TiAl_3$ MMC via squeeze casting of a TiO_2 preform with an Al-alloy (A356-7 at.% Si). Except for the process and minor temperature differences, the DTA results presented by Hsu et al. possess the same features that were observed in this work.

4.2.3. $(Al–Si)_3Ti$

Rapid solidification of induction melted Al–3.87Ti–0.34Si resulted in the formation of Al_3Ti structures that contained Si.[21] In the stable $D0_{22}$-Al_3Ti form, Si replaces the Al atom at the (0, 0, 0.5) generating site.[14]

Based on the observed shifts in the XRD reflections positions of the Al_3Ti derivative phase, SAD that were recorded using TEM, and quantitative EDS data (SEM and TEM), a modified model (see Table 3) based on the $D0_{22}$-Al_3Ti[22] phase is suggested for the $(Al–Si)_3Ti$ structure. The elemental composition was found to be $Al_{60}Si_{12}Ti_{28}$. The crystallographic unit cell parameters are $a = 3.7795$ Å and $c = 8.5209$ Å. The unit cell parameters were estimated according to the characteristic reflecting plane and the measured reflection position (based on XRD). The variation in occupancy was based on the measured composition of the phase ($Al_{60}Si_{12}Ti_{28}$). The elemental composition differs only slightly from the model suggested in the literature[14] ($A1_{12}Si_3Ti_5$), namely 3 at.% with regard to the Si and Ti atomic concentration, but it substantially differs with respect to the suggested occupancies of the generating sites.

Table 3
Suggested $(Al–Si)_3Ti$ crystallographic structure ($D0_{22}$ related)

Generating site	*x*	*Y*	*Z*	Occupancy	Atom
b2	0	0	0.5	0.5	Si
b2	0	0	0.5	0.5	Al
d4	0	0.5	0.25	0.95	Al
d4	0	0.5	0.25	0.05	Ti
a2	0	0	0	1	Ti

Confirmation of the suggested structure for $(Al–Si)_3Ti$ should be achieved by structure refinement (i.e. Rietveld method). In the present case, the use of a structure refinement procedure is not accurate due to the fact that the alloy used for infiltration contained significant amounts of alloying elements.

According to combined DTA and XRD results, the reaction finalizes at 870 °C and an α-Al_2O_3–$(Al–Si)_3Ti$ IPN microstructure is achieved. The $(Al–Si)_3Ti$ structure is the stable configuration below 1000 °C.

4.2.4. The formation of γ-Al_2O_3 and TiO as an intermediate phase

Pan et al.[23] analysed the formation of γ-Al_2O_3 and TiO as intermediate phases during the reduction of TiO_2 whiskers by Al. They identified γ-Al_2O_3 particles (60–70 nm) in the Al matrix and a continuous layer of TiO (10–20 nm) by HRTEM. According to TEM (see Fig. 5) and XRD results, TiO_2 is reduced by Al and forms TiO and Ti_2O_3 polymorphs. The formation of the different titanium oxides is probably due to the complex nature of the Ti–O binary phase diagram.[13] The size of the TiO particle (≈1 μm) and the Ti_2O_3 grains (≈200 nm) is much larger than the dimensions observed by Pan et al.[23] TiO and γ-Al_2O_3 are formed after infiltration of the preform (sample E2, see Fig. 5 and Table 2) and are present to a small extent at high temperatures (sample B2, see Fig. 10). TiO and γ-Al_2O_3 are formed during the reduction of TiO_2 by pure Al.[11] The presence of TiO at high temperatures after thermal annealing (sample B2, see Fig. 10) strengthens the assumption that TiO serves as an intermediate phase in the formation of Al_3Ti.

γ-Al_2O_3 was not detected in sample B2 due to the γ–α alumina transformation. The phase transformation from γ-Al_2O_3 to α-Al_2O_3 is related to a rearrangement of the constituent ions. The transformation occurs at elevated temperatures (700–1100 °C),[24] and the phase transition is accompanied by the formation of porosity, which is related to the volume difference between the two polymorphs. It has

been suggested[24] that the transition is an indirect transition; different intermediate phases are formed in the course of the transformation.

γ-Al_2O_3 is present in the as-infiltrated specimen (see Fig. 6 and Table 2). At this stage, α-Al_2O_3 is already present in the Al matrix. The formation of γ-Al_2O_3 is accompanied by the transformation to α-Al_2O_3, which is probably due to the high temperatures that evolve in the specimen as the reduction reaction takes place. These temperatures initiated the γ–α alumina transformation process. It can be postulated that γ-Al_2O_3 is formed after the reduction of TiO and transforms immediately to α-Al_2O_3. This can only be confirmed by HRTEM analysis of samples that were annealed at different temperatures.

5. Summary and conclusions

The interpenetrating network microstructure and different reactions which occur during the formation of $(Al–Si)_3Ti$–α-Al_2O_3 CMC were investigated. The CMC was formed by squeeze casting of Al-alloys into a ceramic perform, and subsequent heat treatments.

The ceramic preform was formed by the partial sintering of α-Al_2O_3 and TiO_2. The preform is highly reactive due to its low density (high surface area). Pressure infiltration was successful in introducing the liquid alloy into the preform without infiltration defects.

The formation of $(Al–Si)_3Ti$ derives from the consumption of intermediate phases (TiO and γ-Al_2O_3). These intermediate phases are formed by the reduction of TiO_2. The exothermic reaction motivates the transformation of Al_2O_3 polymorphs, and the intensity of the overall reaction. A satisfactory crystallographic model was presented to explain the nature of the $(Al–Si)_3Ti$ ($Al_{60}Si_{12}Ti_{28}$) intermetallic that was formed during the process.

Acknowledgements

The authors wish to thank G. Levi and A. Tvetkov for their technical assistance and discussions. S.A. was partially supported by a Technion stipend.

References

1. Knechtel, M., Prielipp, H., Mullejans, H., Claussen, N. and Rodel, J., Mechanical properties of Al/Al_2O_3 and Cu/Al_2O_3 composites with interpenetrating networks. *Scripta Metall. Mater.*, 1994, **31**(8), 1085–1090.
2. Sternitzke, M., Knechtel, M., Hoffman, M., Broszeit, E. and Rodel, J., Wear properties of alumina/aluminum composites with interpenetrating networks. *J. Am. Ceram. Soc.*, 1996, **79**(1), 121–128.
3. Hillig, W. B., Raddatz, O., Schneider, A. and Claussen, N., Analysis and model of the crack bridging mechanisms in a ductile fiber reinforced ceramic composite. *J. Mater. Sci.*, 2001, **36**, 1653–1663.
4. Schicker, S., Garcia, D. E., Bruhn, J., Janssen, R. and Claussen, N., Reaction synthesized Al_2O_3-based intermetallics composites. *Acta Mater.*, 1998, **46**(7), 2485–2492.
5. Dorre, E. and Hubner, H., *Alumina*. Springer-Verlag, 1984.
6. Peng, H. X., Wang, D. Z., Geng, L., Yao, C. K. and Wang, L. G., SHS process of a dense TiO_2/Al for Al_3Ti-Al_2O_3-Al in situ composite. *Int. J. Self-Propag. High-Temp. Synth.*, 1996, **5**(3), 285–292.
7. Loehman, R. E., Ewsuk, K. and Tomasia, A. P., Synthesis of Al_2O_3-Al composites by reactive metal penetration. *J. Am. Ceram. Soc.*, 1996, **79**(1), 27–32.
8. Wagner, F., Garcia, D. E., Krupp, A. and Claussen, N., Interpenetrating Al_2O_3–$TiAl_3$ alloys produced by reactive infiltration. *J. Eur. Ceram. Soc.*, 1999, **19**, 2449–2453.
9. Beyer, P., Janssen, R. and Claussen, N., Synthesis of aluminide-alumina composites by reactive squeeze casting. *Adv. Eng. Mater.*, 2000, **2**(11), 734–737.
10. Gaus, S. P., Harmer, M. P., Chan, H. M., Caram, H. S., Bruhn, J. and Claussen, N., Alumina-aluminide alloys (3a) technology. II. Modeling of Ti_x-Al_y-Al_2O_3 composites formation. *J. Am. Ceram. Soc.*, 2000, **83**(7), 1606–1612.
11. Feng, C. F. and Froyen, L., Formation of Al_3Ti and Al_2O_3 from an Al-TiO_2 system for preparing in situ aluminum matrix composites. *Composites: Part A*, 2000, **31**, 385–390.
12. JCPDF card No. 37-1449, The International Centre for Diffraction Data, 1999.
13. Wriedt, H. A. and Muarray, J. L., ed., *The O–Ti (Oxygen–Titanium) System, Phase Diagrams of Binary Titanium Alloys*. ASM International Metal Park, 1987, pp. 211–229.
14. Villars, P. and Calvert, L. D., *Pearson's Handbook of Crystallographic Data for Intermetallics Phases* (2*nd ed.*). ASM-International, 1991.
15. German, R. M., *Sintering-Theory and Practice*. Wiley-Interscience, 1996.
16. Trumble, K. P., Spontaneous infiltration of non-cylindrical porosity: close-packed spheres. *Acta Mater.*, 1998, **46**(7), 2363–2367.
17. Laurent, V., Chatain, D., Chatillon, C. and Eustathopoulos, N., Wettability of monocrystalline alumina by aluminum between its melting point and 1273 K. *Acta Metall.*, 1988, **36**(7), 1797–1803.
18. Avraham, S. and Kaplan, W. D., Reactive wetting of rutile by liquid aluminium. *J. Mater. Sci.*, 2005, **40**(5), 1093–1100.
19. Hsu, C. W. and Chao, C. G., Effect of heat treatments on in situ Al_2O_3/$TiAl_3$ composites produced from squeeze casting of TiO_2/A356 composite. *Metall. Mater. Trans. B*, 2002, **33B**, 31–40.
20. Muarray, J. L. and Mcalister, A. J., In *Al–Si (Aluminium–Silicon), Binary Alloy Phase Diagrams*, ed. T. B. Massalsi. ASM international, Metals Park, 1986, pp. 164–167.
21. You, B. Y. and Park, W. W., Age hardening phenomena and microstructure of rapidly solidifies Al–Ti–Si and Al–Cr–Y Alloys. *Scripta Mater.*, 1996, **34**(2), 201–205.
22. JCPDS card No. 37-1449, The International Centre for Diffraction Data, 1999.
23. Pan, J., Li, J. H., Fukunaga, H., Ning, X. G., Ye, H. Q., Yao, Z. K. *et al.*, Microstructural study of the interface reaction between titania whiskers and aluminium. *Comp. Sci. Tech.*, 1997, **57**, 319–325.
24. Levin, I. and Brandon, D., Metastable alumina polymorphs: crystal structure and transition sequences. *J. Am. Ceram. Soc.*, 1998, **81**(8), 1995–2012.